Electronic Supplementary Information

Highly Efficient Room-Temperature Organic Afterglow Achieved by Collaboration of Luminescent Dimeric TADF Dopants and Rigid Matrices

Bei Zhou, Guangming Wang, Xuepu Wang, Wang Guo, Junbo Li, and Kaka Zhang*

Key Laboratory of Synthetic and Self-Assembly Chemistry for Organic Functional Molecules, Shanghai Institute of Organic Chemistry, University of Chinese Academy of Sciences, Chinese Academy of Sciences, 345 Lingling Road, Shanghai 200032, People's Republic of China.

*Email: zhangkaka@sioc.ac.cn

Table of Contents

Fig. S27 Photographs of samples prepared by doping 1.0 wt% 530 into solid paraffin under 365 nm UV lamp and after removal of 365 nm UV lamp at room temperature

Text S1. Optimization of excitation wavelength for PLQY measurement

Table S1. Crystal data and structure refinement for mo_d8v20460_0m

Table S2. Atomic coordinates and equivalent isotropic displacement parameters for mo_d8v20460_0m

Table S3. Bond lengths [Å] and angles [°] for mo_d8v20460_0m

Physical measurements and instrumentation

^{1}H NMR (400 MHz), ^{13}C{^{1}H} NMR (100 MHz), ^{19}F NMR (376 MHz) and ^{11}B NMR (128 MHz) spectra were recorded on a JEOL Fourier-transform NMR spectrometer (400 MHz). Mass spectra were performed on Agilent Technologies 5973N and Thermo Fisher Scientific LTQ FT Ultras mass spectrometer. FT-IR spectra were recorded on a Nicolet AVATAR-360 FT-IR spectrophotomerter with a resolution of 4 cm^{-1}. Differential scanning calorimetry (DSC) was performed on a TA Q200 DSC instrument in nitrogen with a heating rate of 20 ℃/min. Elemental analysis was carried out on a Carlo-Erba1106 system. UV-Vis absorption spectra were recorded on a Hitachi U-3310 UV-vis spectrophotometer and a Techcomp UV1050 UV-vis spectrophotometer. Emission spectra were recorded using Edinburgh FLS1000 fluorescence spectrometer, Hitachi FL-7000 fluorescence spectrometer and Horiba FluoroLog-3 fluorescence spectrometer. Photoluminescence quantum yield was measured by a Hamamatsu absolute PL quantum yield measurement system based on a standard protocol.[S1] Single-crystal X-ray diffraction analysis was performed on a D8 VENTURE SC-XRD instrument. Photographs and videos were captured by a iPhone 11 camera. Before imaging, samples were irradiated by a 365 nm UV lamp (5 W) for approximately 5 s at a distance of approximately 10 cm. Grey value analysis was performed by a Image J 1.52a software using plot profile function. All animal procedures were reviewed and approved by the Institutional Animal Care and Use Committee at Chinese Academy of Sciences and are in accordance with the Guide for the Care and Use of Laboratory Animals of Chinese Academy of Sciences. TD-DFT calculations were performed on Gaussian 16 software with B3LYP functional and 6-31G(d) basis set.[S2] The single crystal structure of 530 was used as the ground state geometry. To maintain the specific molecular configurations and corresponding intermolecular locations, only H atoms were optimized and no further optimization was conducted.
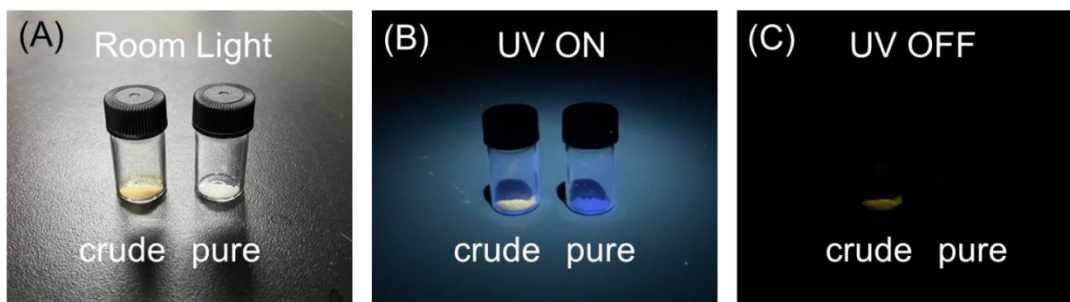
Fig. S1 Photographs of crude tetralone-3 powder and purified tetralone-3 powder (A) in room light, (B) under 365 nm UV lamp and (C) 0.2 s after removal of 365 nm UV lamp. Tetralone-3 was purified by careful column chromatography over silica gel (300-400 mesh) using petroleum ether/ethyl acetate (25:1) as eluent.
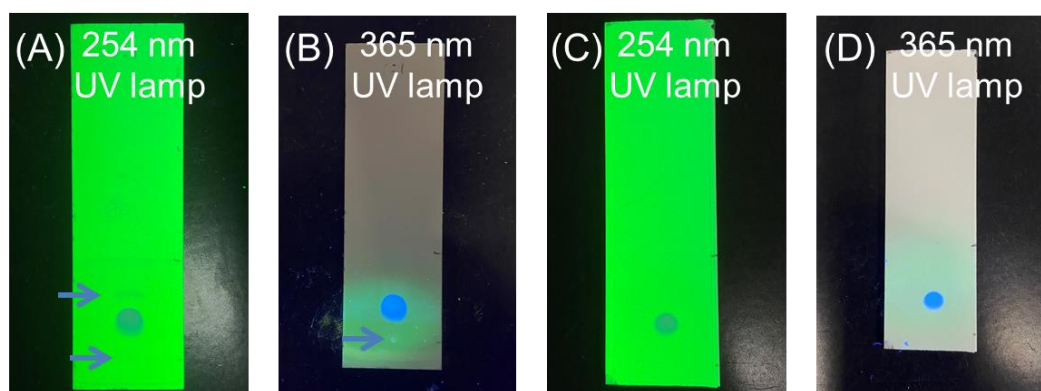
Fig. S2 Thin-layer chromatography of (A and B) the crude tetralone-3 and (C and D) purified tetralone-3 under 254 nm UV lamp and 365 nm UV lamp. The arrows indicate the impurities.
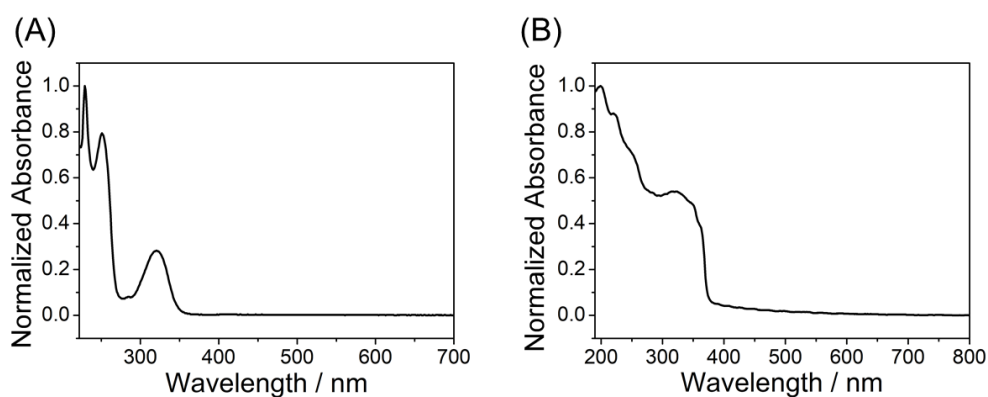
Fig. S3 UV-Vis spectra of (A) ethanol solution of the purified tetralone-3 and (B) the crystalline solids of the purified tetralone-3.
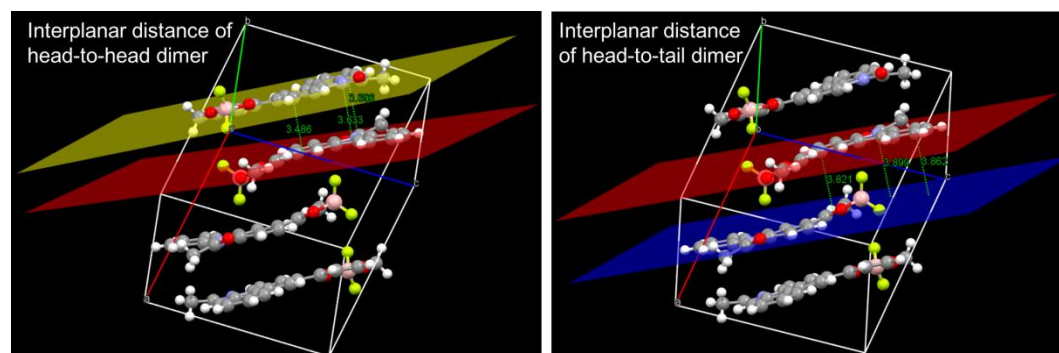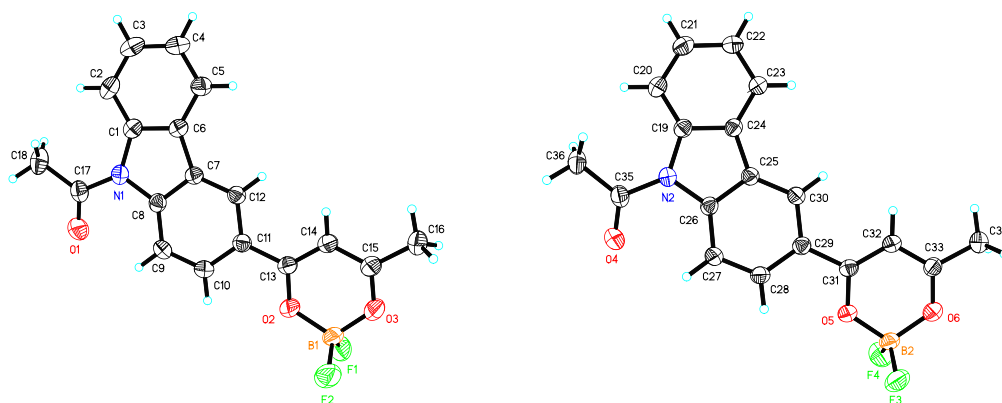
Fig. S4 Single-crystal structures of 530. Interplanar distances have been indicated (unit, Å).
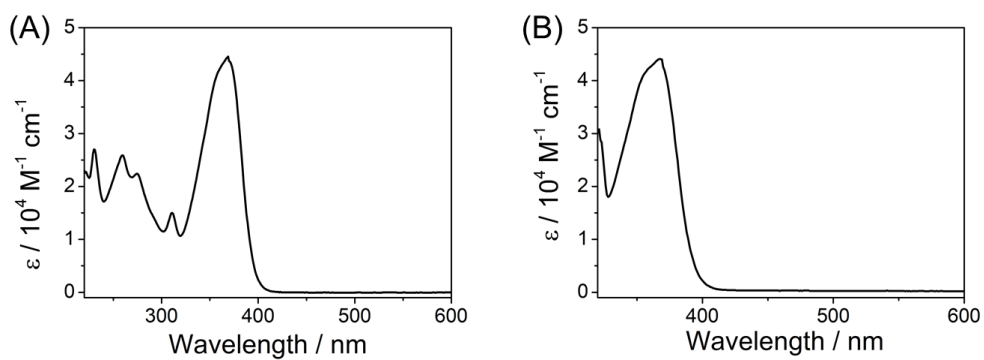
Fig. S5 UV-Vis spectra of 530 (A) in dichloromethane and (B) in acetone.
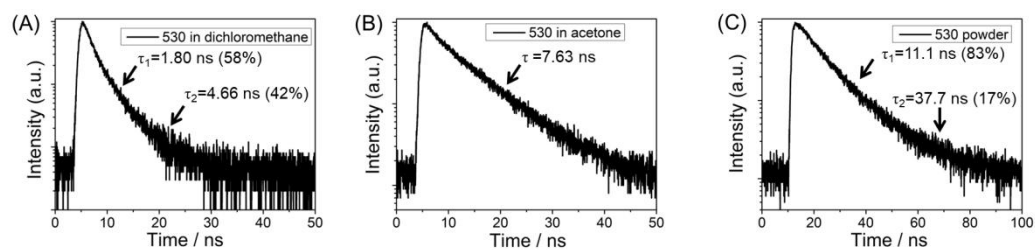
Fig. S6 Room-temperature emission decay of (A) 530 solution in dichloromethane, (B) 530 solution in acetone, and (C) 530 powder.
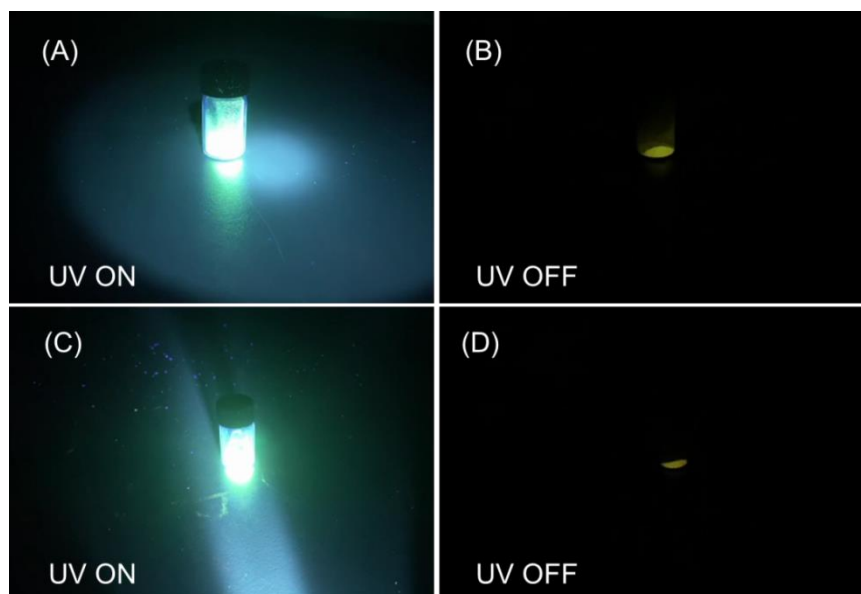
Fig. S7 Photographs of (A, UV on; B, UV off) 530-3-5% solids and (C, UV on; D, UV off) 530-3-10% solids.
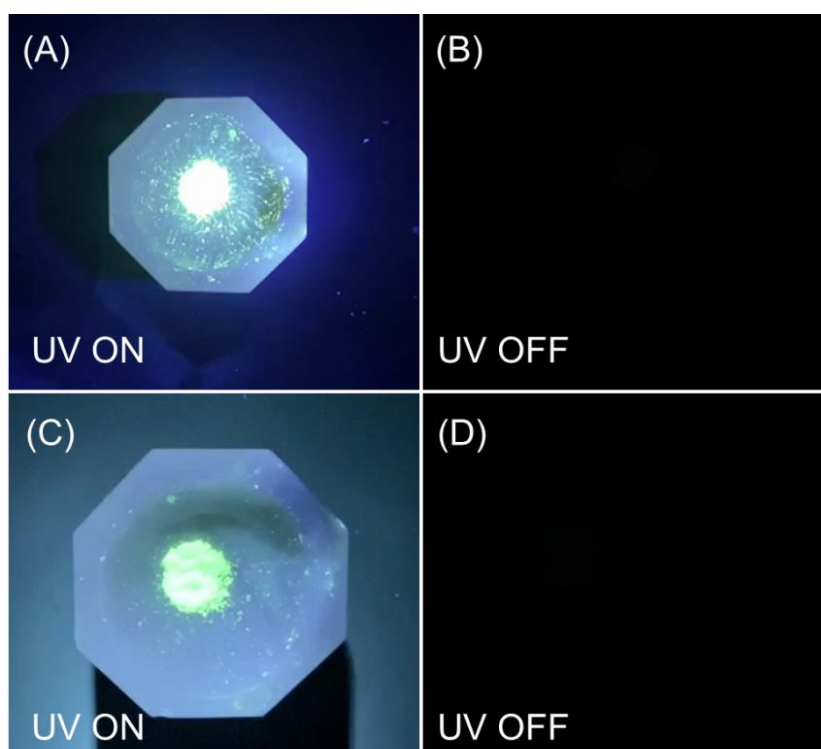
Fig. S8 Photographs of (A, UV on; B, UV off) 530-3-0.1% solids and (C, UV on; D, UV off) 530-3-0.5% solids.
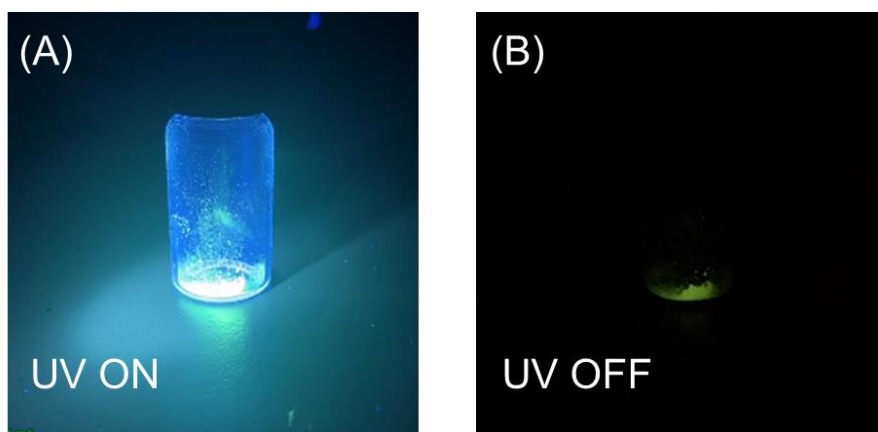
Fig. S9 Photographs of 530-4-1% solids (A) under 365 nm UV lamp and (B) after removal of 365 nm UV lamp.
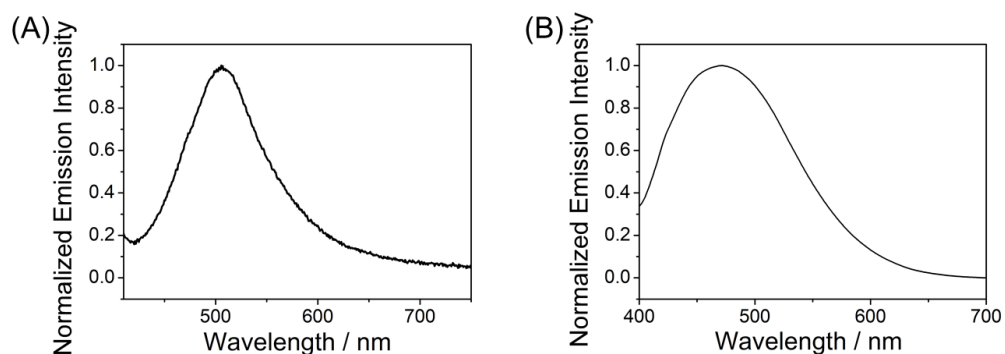
Fig. S10 Room-temperature steady-state emission spectra of (A) 530-3-10% solid samples and (B) 530-3-0.1% solid samples.
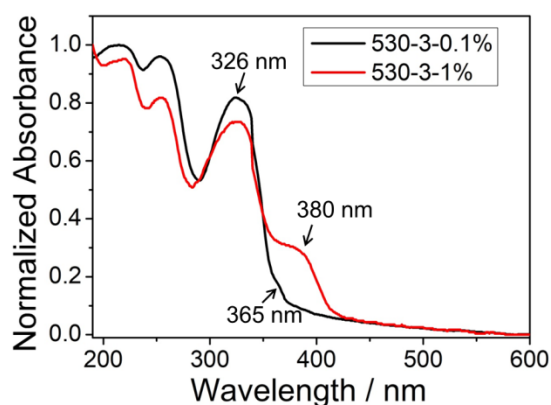
Fig. S11 UV-Vis spectra of 530-3-0.1% and 530-3-1% thin films. The thin films were prepared by sandwiching a hot melt of 530-3 mixture between two 1 cm × 4 cm quartz plates. Tetralone-3 matrices show absorption bands at 326 nm. 530-3-0.1% thin films show absorption signal at 365 nm. 530-3-1% thin films exhibit a red-shifted absorption band at 380 nm, which suggest the aggregation of 530 molecules in 530-3-1% solid samples.
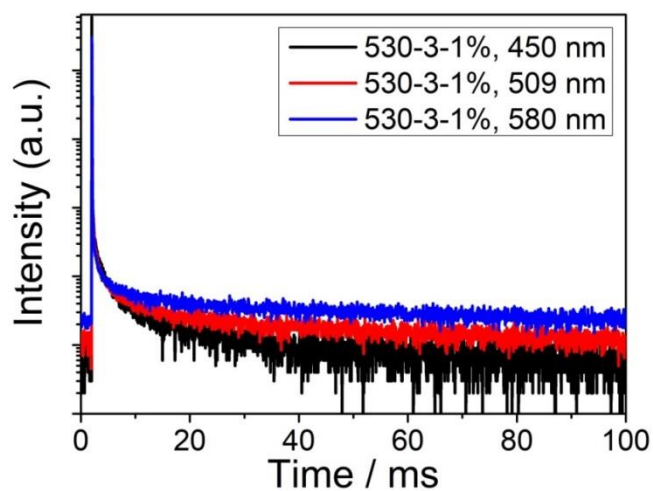
Fig. S12 Room-temperature emission decay of 530-3-1% solids excited at 365 nm in the time range of 0 to 100 ms monitored at emission onset (450 nm), maxima (509 nm) and tail (580 nm). The emission decay curves monitored at emission onset (450 nm), maxima (509 nm) and tail (580 nm) show similar decay behaviors, which suggests that the emission band in the range of 450 to 580 nm are originated from the same excited state.
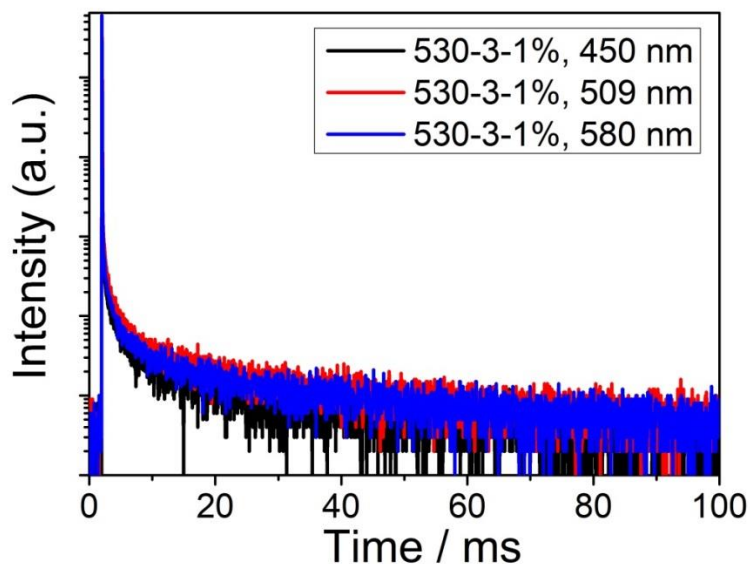
Fig. S13 Room-temperature emission decay of 530-3-1% solids excited at 405 nm in the time range of 0 to 100 ms monitored at emission onset (450 nm), maxima (509 nm) and tail (580 nm). The emission decay curves monitored at emission onset (450 nm), maxima (509 nm) and tail (580 nm) show similar decay behaviors, which suggests that the emission band in the range of 450 to 580 nm are originated from the same excited state.
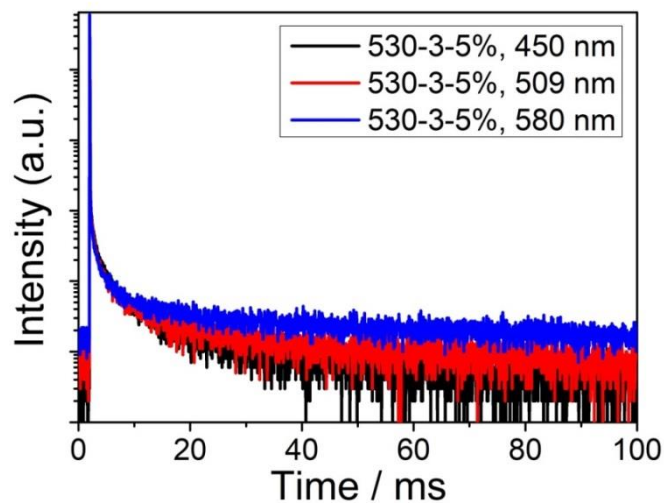
Fig. S14 Room-temperature emission decay of 530-3-5% solids excited at 365 nm in the time range of 0 to 100 ms monitored at emission onset (450 nm), maxima (509 nm) and tail (580 nm). The emission decay curves monitored at emission onset (450 nm), maxima (509 nm) and tail (580 nm) show similar decay behaviors, which suggests that the emission band in the range of 450 to 580 nm are originated from the same excited state.
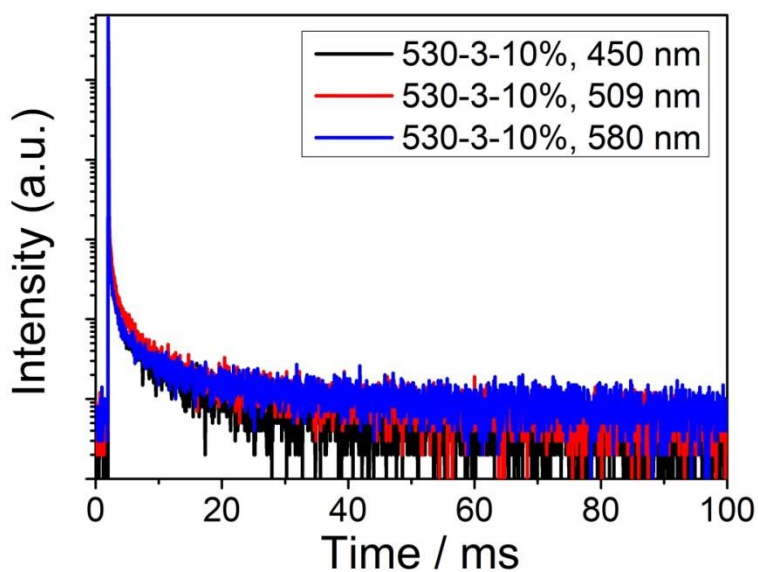
Fig. S15 Room-temperature emission decay of 530-3-10% solids excited at 365 nm in the time range of 0 to 100 ms monitored at emission onset (450 nm), maxima (509 nm) and tail (580 nm). The emission decay curves monitored at emission onset (450 nm), maxima (509 nm) and tail (580 nm) show similar decay behaviors, which suggests that the emission band in the range of 450 to 580 nm are originated from the same excited state.
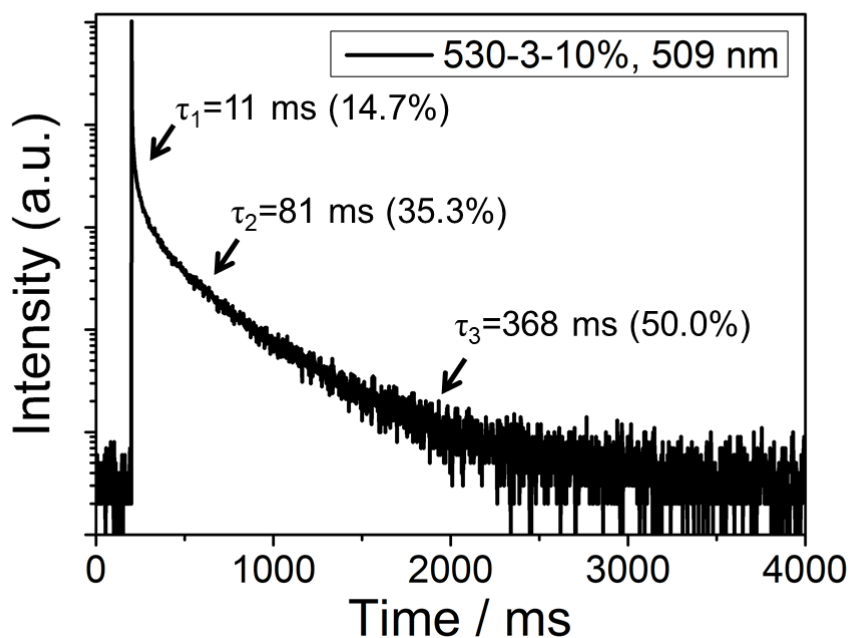
Fig. S16 Room-temperature emission decay of 530-3-10% solids in the range of 0 to 4000 ms excited at 365 nm. The $\tau_2 = 81$ ms (35.3%) and $\tau_3 = 368$ ms (50.0%) parts in the decay curves of the 530-3-10% solid samples are responsible for the afterglow phenomenon observed in the present study.The absolute PLQY of 530-3-10% solids is determined to be 30±1%, and thus the afterglow quantum yield of 530-3-10% solids can be calculated to be 26±1%.
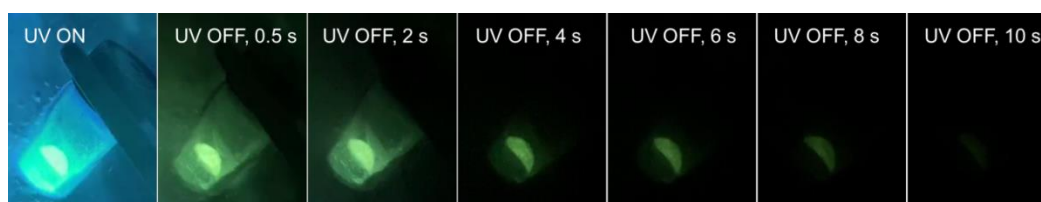
Fig. S17 Photographs of 530-3-1% solids at 77 K under 365 nm UV lamp and after removal of 365 nm UV lamp.

Fig. S18 Photographs of 530 solids at 77 K under 365 nm UV lamp and after removal of 365 nm UV lamp.

530 monomer

S_1
3.5981 eV
$f_{osc} = 0.0092$

T_1
2.7899 eV
$f_{osc} = 0.0000$

S_0

530 dimer

S_1
3.3505 eV
$f_{osc} = 0.0000$

T_1
2.7405 eV
$f_{osc} = 0.0000$

S_0
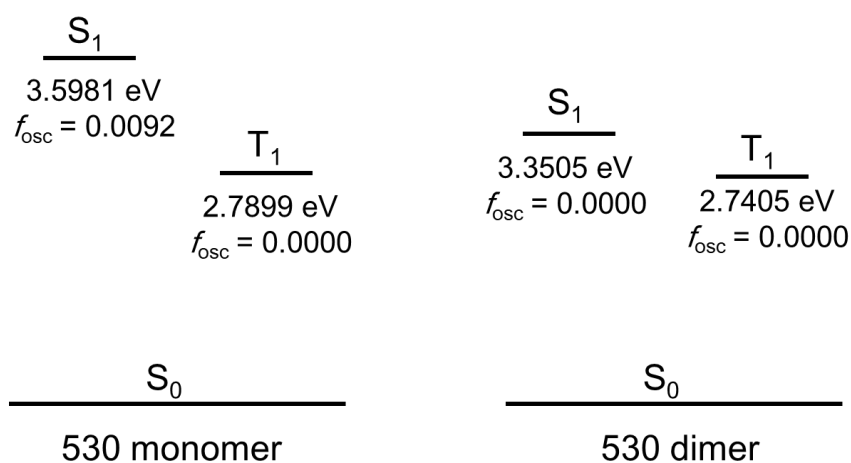
Fig. S19 Lowest excited singlet and triplet levels obtained by TD-DFT calculations.
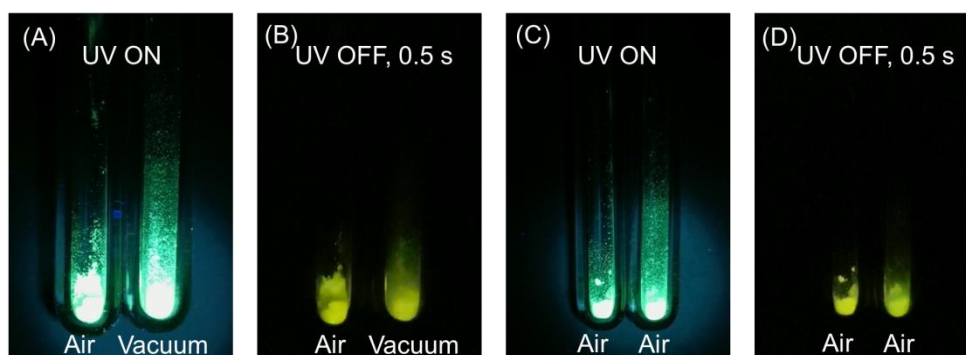
Fig. S20 (A, B) Photographs of 530-3-1% solid samples in air (left quartz tube) and under vacuum (right quartz tube) before and after removal of 365 nm UV lamp. (C, D) By exposing the right quartz tube to air, the photographs of 530-3-1% solid samples before and after removal of 365 nm UV lamp were captured again.

Fig. S21 The traditional preparation procedures for Chinese New Year Cake in Ningbo, Zhejiang Province. Grinding (A) rice into (B) aqueous suspension by a mill with the aid of water is a defining procedure for making (C) Chinese New Year Cake in Ningbo.
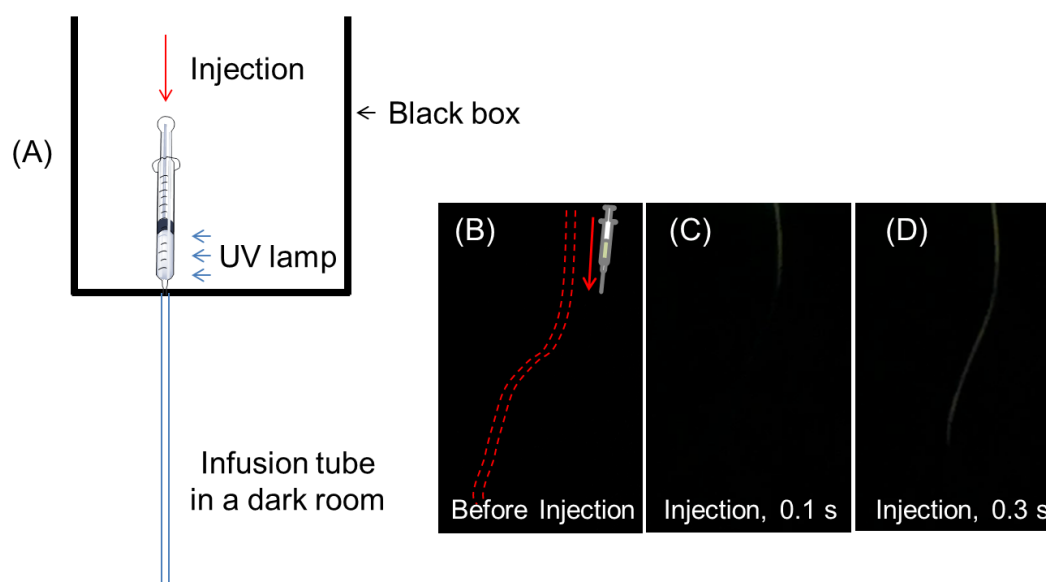
Fig. S22 (A) Schematic illustration shows that the 530-3-1% aqueous suspension was first activated by UV light in a black box and then the afterglow suspension was injected into an infusion tube in a dark room. (B) Photographs recorded in a dark room during the injection of 530-3-1% aqueous suspension into an infusion tube. Arrow indicates the direction of injection. The 530-3-1% afterglow suspension is capable of imaging the infusion tube in a dark environment.
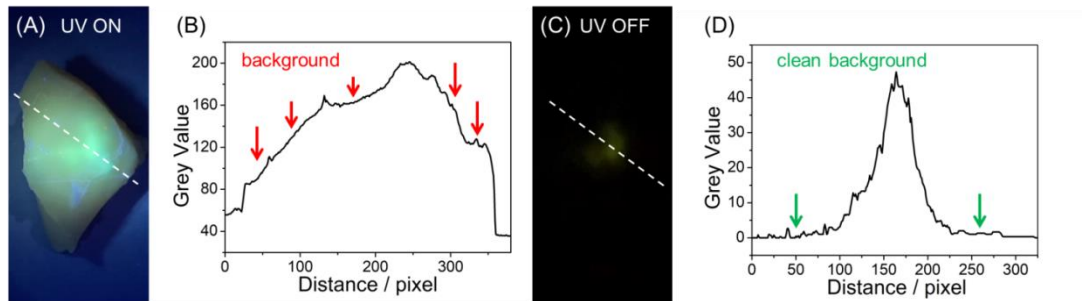
Fig. S23 Bioimaging of chicken breast by 530-3-1% aqueous suspension (A) under 365 nm UV lamp and (C) after removal of UV lamp. (B) Grey values along the dashed line in (A) show the presence of background interference indicated by red arrows. (D) Grey values along the dashed line in (C) show clean background in the afterglow image.
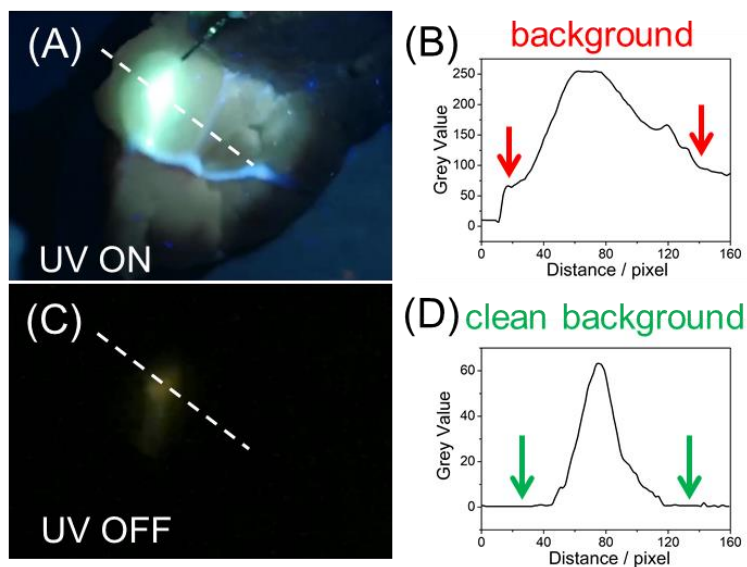
Fig. S24 Bioimaging of pork by 530-3-1% aqueous suspension (A) under 365 nm UV lamp and (C) after removal of UV lamp. (B) Grey values along the dashed line in (A) show the presence of background interference indicated by red arrows. (D) Grey values along the dashed line in (C) show clean background in the afterglow image.
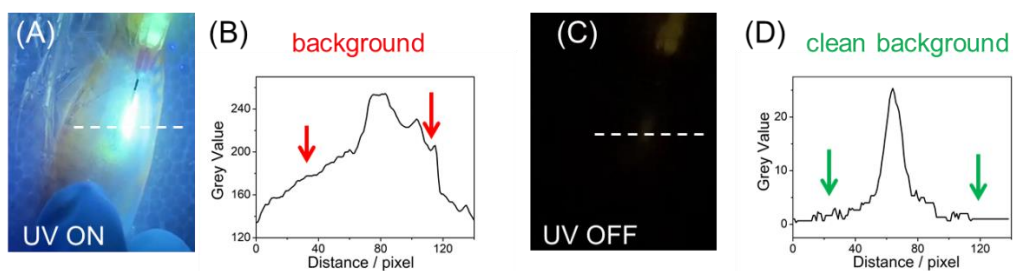
Fig. S25 Bioimaging of living fish by 530-3-1% aqueous suspension (A) under 365 nm UV lamp and (C) after removal of UV lamp. (B) Grey values along the dashed line in (A) show the presence of background interference indicated by red arrows. (D) Grey values along the dashed line in (C) show clean background in the afterglow image
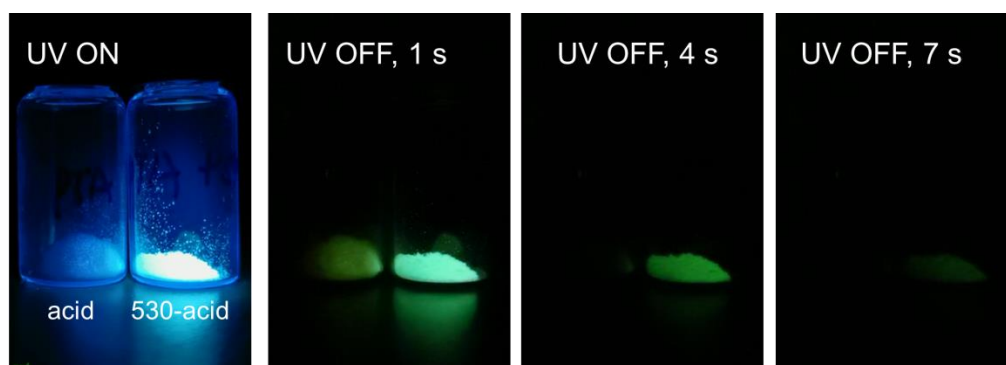
Fig. S26 Photographs of 1,3,5-benzenetricarboxylic acid (BTA) and 530-BTA-1% solids under 365 nm UV lamp and after removal of 365 nm UV lamp. The BTA powders show weak room-temperature afterglow that can last for about 3 s, while 530-BTA-1% solids show strong afterglow that can last for about 7 s.
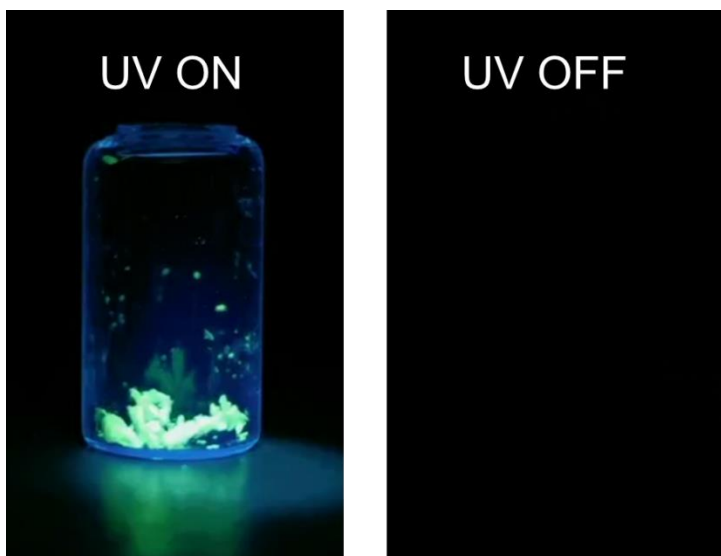
Fig. S27 Photographs of samples prepared by doping 1.0 wt% 530 into solid paraffin under 365 nm UV lamp and after removal of 365 nm UV lamp at room temperature. No afterglow property was observed.

Text S1. The result that the PLQY of 530-3-5% and 530-3-10% is higher than that of 530-3-1% is caused by the UV-vis absorption of tetralone-3 matrices. We first selected 365 nm for the excitation of 530-3-1% samples to obtain a PLQY as low as 5.8%. Tetralone-3 matrices can absorb a large percent of the energy of the 365 nm excitation source but give little emission. Then, excitation wavelength was optimized at 390 nm for PLQY measurement to not only minimize the absorption of tetralone-3 but also ensure the integration of the whole emission spectra. A small amount of the 390 nm excitation source can still be absorbed by tetralone-3 matrices since the excitation source is not monochromatic but has a certain width of wavelength distribution. It is apparent that the percent of the absorbed energy by tetralone-3 matrices decreases with 530 doping concentrations since 530 has intense absorption at 390 nm. Therefore, the PLQY of 530-3 materials increases with 530 doping concentration.

Table S1. Crystal data and structure refinement for mo_d8v20460_0m.

Identification code	mo_d8v20460_0m	
Empirical formula	C18 H14 B F2 N O3	
Formula weight	341.11	
Temperature	293(2) K	
Wavelength	0.71073 Å	
Crystal system	Triclinic	
Space group	P -1	
Unit cell dimensions	a = 11.9793(6) Å	α= 113.6570(10) °.
	b = 12.4354(5) Å	β= 105.751(2) °.
	c = 12.6474(6) Å	γ = 02.8960(10) °.
Volume	1538.55(12) Å^3	
Z	4	
Density (calculated)	1.473 Mg/m^3	
Absorption coefficient	0.115 mm^{-1}	
F(000)	704	
Crystal size	0.190 x 0.160 x 0.110 mm^3	
Theta range for data collection	2.996 to 25.500 °.	
Index ranges	-14<=h<=14, -15<=k<=15, -15<=l<=15	
Reflections collected	36633	
Independent reflections	5700 [R(int) = 0.0471]	
Completeness to theta = 25.242 °	99.5 %	
Absorption correction	Semi-empirical from equivalents	
Max. and min. transmission	0.7456 and 0.7002	
Refinement method	Full-matrix least-squares on F^2	
Data / restraints / parameters	5700 / 0 / 456	
Goodness-of-fit on F^2	1.058	
Final R indices [I>2sigma(I)]	R1 = 0.0575, wR2 = 0.1625	
R indices (all data)	R1 = 0.0775, wR2 = 0.1799	
Extinction coefficient	0.016(3)	
Largest diff. peak and hole	0.196 and -0.192 e.Å^{-3}	

Table S2. Atomic coordinates (x 10^4) and equivalent isotropic displacement parameters (Å^2x 10^3) for mo_d8v20460_0m. U(eq) is defined as one third of the trace of the orthogonalized U^{ij} tensor.

	x	y	z	U(eq)
F(1)	-775(2)	1936(2)	-1039(2)	90(1)
F(2)	951(3)	1886(2)	160(2)	110(1)
O(1)	-693(3)	7019(3)	6093(3)	87(1)
O(2)	426(2)	3631(2)	956(2)	73(1)
O(3)	1153(2)	3151(2)	-747(2)	75(1)
N(1)	563(2)	8269(2)	5647(2)	53(1)
C(1)	1180(2)	9424(3)	5699(3)	51(1)
C(2)	1361(3)	10672(3)	6481(3)	66(1)
C(3)	1973(3)	11596(3)	6267(3)	71(1)
C(4)	2387(3)	11308(3)	5304(3)	66(1)
C(5)	2194(3)	10076(3)	4520(3)	57(1)
C(6)	1585(2)	9130(2)	4716(3)	48(1)
C(7)	1222(2)	7772(2)	4038(2)	45(1)
C(8)	581(2)	7264(3)	4612(2)	49(1)
C(9)	124(3)	5965(3)	4161(3)	58(1)
C(10)	306(3)	5196(3)	3138(3)	56(1)
C(11)	927(2)	5683(3)	2537(3)	49(1)
C(12)	1391(2)	6989(2)	3005(2)	47(1)
C(13)	1049(3)	4824(3)	1419(3)	50(1)
C(14)	1744(3)	5206(3)	836(3)	61(1)
C(15)	1766(3)	4354(3)	-242(3)	58(1)
C(16)	2453(3)	4729(3)	-927(3)	72(1)
C(17)	-21(3)	8076(3)	6417(3)	60(1)
C(18)	219(3)	9191(4)	7626(3)	78(1)
B(1)	430(4)	2622(3)	-175(3)	66(1)
F(3)	4704(2)	4945(2)	1398(2)	88(1)
F(4)	6288(2)	5143(2)	2991(2)	87(1)
O(4)	5501(3)	11766(2)	7816(2)	81(1)
O(5)	4821(2)	5961(2)	3425(2)	64(1)
O(6)	4325(2)	3681(2)	2290(2)	67(1)
N(2)	4267(2)	10158(2)	7899(2)	46(1)
C(19)	3671(2)	9602(2)	8489(2)	45(1)
C(20)	3495(3)	10134(3)	9598(3)	57(1)

C(21)	2905(3)	9323(3)	9941(3)	62(1)
C(22)	2505(3)	8018(3)	9232(3)	61(1)
C(23)	2714(3)	7489(3)	8153(3)	54(1)
C(24)	3298(2)	8280(2)	7779(2)	44(1)
C(25)	3681(2)	8015(2)	6746(2)	43(1)
C(26)	4283(2)	9178(2)	6847(2)	43(1)
C(27)	4751(3)	9224(3)	5963(3)	49(1)
C(28)	4636(3)	8100(3)	5022(3)	49(1)
C(29)	4077(2)	6922(2)	4928(2)	44(1)
C(30)	3574(2)	6886(2)	5792(2)	44(1)
C(31)	4102(2)	5770(2)	3981(2)	44(1)
C(32)	3462(3)	4558(3)	3706(3)	54(1)
C(33)	3610(3)	3543(3)	2868(3)	49(1)
C(34)	2990(3)	2224(3)	2576(3)	60(1)
C(35)	4809(3)	11451(3)	8263(3)	56(1)
C(36)	4487(3)	12387(3)	9191(3)	67(1)
B(2)	5049(4)	4937(3)	2505(3)	58(1)

_____

Table S3. Bond lengths [Å] and angles [°] for mo_d8v20460_0m.

_____

F(1)-B(1)	1.361(4)
F(2)-B(1)	1.353(4)
O(1)-C(17)	1.209(4)
O(2)-C(13)	1.293(3)
O(2)-B(1)	1.479(4)
O(3)-C(15)	1.294(4)
O(3)-B(1)	1.474(5)
N(1)-C(17)	1.406(4)
N(1)-C(8)	1.411(3)
N(1)-C(1)	1.427(4)
C(1)-C(2)	1.390(4)
C(1)-C(6)	1.399(4)
C(2)-C(3)	1.384(5)
C(2)-H(2)	0.9300
C(3)-C(4)	1.383(5)
C(3)-H(3)	0.9300
C(4)-C(5)	1.372(4)
C(4)-H(4)	0.9300
C(5)-C(6)	1.388(4)
C(5)-H(5)	0.9300
C(6)-C(7)	1.444(4)
C(7)-C(12)	1.380(4)
C(7)-C(8)	1.404(4)
C(8)-C(9)	1.390(4)
C(9)-C(10)	1.374(4)
C(9)-H(9)	0.9300
C(10)-C(11)	1.405(4)
C(10)-H(10)	0.9300
C(11)-C(12)	1.394(4)
C(11)-C(13)	1.460(4)
C(12)-H(12)	0.9300
C(13)-C(14)	1.379(4)
C(14)-C(15)	1.362(4)
C(14)-H(14)	0.9300
C(15)-C(16)	1.478(4)
C(16)-H(16A)	0.9600

C(16)-H(16B)	0.9600
C(16)-H(16C)	0.9600
C(17)-C(18)	1.491(5)
C(18)-H(18A)	0.9600
C(18)-H(18B)	0.9600
C(18)-H(18C)	0.9600
F(3)-B(2)	1.353(4)
F(4)-B(2)	1.362(4)
O(4)-C(35)	1.203(4)
O(5)-C(31)	1.290(3)
O(5)-B(2)	1.479(4)
O(6)-C(33)	1.293(3)
O(6)-B(2)	1.480(4)
N(2)-C(26)	1.407(3)
N(2)-C(35)	1.413(3)
N(2)-C(19)	1.424(3)
C(19)-C(20)	1.388(4)
C(19)-C(24)	1.407(4)
C(20)-C(21)	1.380(4)
C(20)-H(20)	0.9300
C(21)-C(22)	1.386(4)
C(21)-H(21)	0.9300
C(22)-C(23)	1.377(4)
C(22)-H(22)	0.9300
C(23)-C(24)	1.388(4)
C(23)-H(23)	0.9300
C(24)-C(25)	1.439(4)
C(25)-C(30)	1.385(3)
C(25)-C(26)	1.401(3)
C(26)-C(27)	1.395(4)
C(27)-C(28)	1.371(4)
C(27)-H(27)	0.9300
C(28)-C(29)	1.410(4)
C(28)-H(28)	0.9300
C(29)-C(30)	1.395(3)
C(29)-C(31)	1.465(4)
C(30)-H(30)	0.9300
C(31)-C(32)	1.378(4)

C(32)-C(33)	1.370(4)
C(32)-H(32)	0.9300
C(33)-C(34)	1.483(4)
C(34)-H(34A)	0.9600
C(34)-H(34B)	0.9600
C(34)-H(34C)	0.9600
C(35)-C(36)	1.494(4)
C(36)-H(36A)	0.9600
C(36)-H(36B)	0.9600
C(36)-H(36C)	0.9600
C(13)-O(2)-B(1)	123.4(3)
C(15)-O(3)-B(1)	122.4(2)
C(17)-N(1)-C(8)	122.8(2)
C(17)-N(1)-C(1)	129.3(2)
C(8)-N(1)-C(1)	107.8(2)
C(2)-C(1)-C(6)	120.2(3)
C(2)-C(1)-N(1)	131.5(3)
C(6)-C(1)-N(1)	108.2(2)
C(3)-C(2)-C(1)	117.8(3)
C(3)-C(2)-H(2)	121.1
C(1)-C(2)-H(2)	121.1
C(2)-C(3)-C(4)	122.0(3)
C(2)-C(3)-H(3)	119.0
C(4)-C(3)-H(3)	119.0
C(5)-C(4)-C(3)	120.3(3)
C(5)-C(4)-H(4)	119.9
C(3)-C(4)-H(4)	119.9
C(4)-C(5)-C(6)	118.9(3)
C(4)-C(5)-H(5)	120.6
C(6)-C(5)-H(5)	120.6
C(5)-C(6)-C(1)	120.7(3)
C(5)-C(6)-C(7)	131.4(3)
C(1)-C(6)-C(7)	107.8(2)
C(12)-C(7)-C(8)	120.6(2)
C(12)-C(7)-C(6)	131.9(3)
C(8)-C(7)-C(6)	107.4(2)
C(9)-C(8)-C(7)	120.4(3)

C(9)-C(8)-N(1)	130.9(3)
C(7)-C(8)-N(1)	108.7(2)
C(10)-C(9)-C(8)	118.4(3)
C(10)-C(9)-H(9)	120.8
C(8)-C(9)-H(9)	120.8
C(9)-C(10)-C(11)	122.1(3)
C(9)-C(10)-H(10)	119.0
C(11)-C(10)-H(10)	119.0
C(12)-C(11)-C(10)	119.0(3)
C(12)-C(11)-C(13)	120.9(2)
C(10)-C(11)-C(13)	120.1(2)
C(7)-C(12)-C(11)	119.5(3)
C(7)-C(12)-H(12)	120.2
C(11)-C(12)-H(12)	120.2
O(2)-C(13)-C(14)	119.7(3)
O(2)-C(13)-C(11)	115.7(3)
C(14)-C(13)-C(11)	124.6(3)
C(15)-C(14)-C(13)	121.4(3)
C(15)-C(14)-H(14)	119.3
C(13)-C(14)-H(14)	119.3
O(3)-C(15)-C(14)	121.2(3)
O(3)-C(15)-C(16)	115.7(3)
C(14)-C(15)-C(16)	123.1(3)
C(15)-C(16)-H(16A)	109.5
C(15)-C(16)-H(16B)	109.5
H(16A)-C(16)-H(16B)	109.5
C(15)-C(16)-H(16C)	109.5
H(16A)-C(16)-H(16C)	109.5
H(16B)-C(16)-H(16C)	109.5
O(1)-C(17)-N(1)	119.6(3)
O(1)-C(17)-C(18)	121.7(3)
N(1)-C(17)-C(18)	118.7(3)
C(17)-C(18)-H(18A)	109.5
C(17)-C(18)-H(18B)	109.5
H(18A)-C(18)-H(18B)	109.5
C(17)-C(18)-H(18C)	109.5
H(18A)-C(18)-H(18C)	109.5
H(18B)-C(18)-H(18C)	109.5

F(2)-B(1)-F(1)	111.1(3)
F(2)-B(1)-O(3)	108.7(3)
F(1)-B(1)-O(3)	108.3(3)
F(2)-B(1)-O(2)	109.0(3)
F(1)-B(1)-O(2)	108.0(3)
O(3)-B(1)-O(2)	111.7(3)
C(31)-O(5)-B(2)	123.7(2)
C(33)-O(6)-B(2)	122.5(2)
C(26)-N(2)-C(35)	122.7(2)
C(26)-N(2)-C(19)	108.0(2)
C(35)-N(2)-C(19)	129.2(2)
C(20)-C(19)-C(24)	120.3(3)
C(20)-C(19)-N(2)	131.8(2)
C(24)-C(19)-N(2)	107.8(2)
C(21)-C(20)-C(19)	117.8(3)
C(21)-C(20)-H(20)	121.1
C(19)-C(20)-H(20)	121.1
C(20)-C(21)-C(22)	122.5(3)
C(20)-C(21)-H(21)	118.8
C(22)-C(21)-H(21)	118.8
C(23)-C(22)-C(21)	119.9(3)
C(23)-C(22)-H(22)	120.1
C(21)-C(22)-H(22)	120.1
C(22)-C(23)-C(24)	119.0(3)
C(22)-C(23)-H(23)	120.5
C(24)-C(23)-H(23)	120.5
C(23)-C(24)-C(19)	120.6(2)
C(23)-C(24)-C(25)	131.6(2)
C(19)-C(24)-C(25)	107.8(2)
C(30)-C(25)-C(26)	120.9(2)
C(30)-C(25)-C(24)	131.6(2)
C(26)-C(25)-C(24)	107.5(2)
C(27)-C(26)-C(25)	120.7(2)
C(27)-C(26)-N(2)	130.4(2)
C(25)-C(26)-N(2)	108.8(2)
C(28)-C(27)-C(26)	117.7(2)
C(28)-C(27)-H(27)	121.1
C(26)-C(27)-H(27)	121.1

C(27)-C(28)-C(29)	122.6(2)
C(27)-C(28)-H(28)	118.7
C(29)-C(28)-H(28)	118.7
C(30)-C(29)-C(28)	119.0(2)
C(30)-C(29)-C(31)	121.0(2)
C(28)-C(29)-C(31)	119.8(2)
C(25)-C(30)-C(29)	118.9(2)
C(25)-C(30)-H(30)	120.5
C(29)-C(30)-H(30)	120.5
O(5)-C(31)-C(32)	120.4(2)
O(5)-C(31)-C(29)	114.9(2)
C(32)-C(31)-C(29)	124.6(2)
C(33)-C(32)-C(31)	120.5(3)
C(33)-C(32)-H(32)	119.8
C(31)-C(32)-H(32)	119.8
O(6)-C(33)-C(32)	121.6(3)
O(6)-C(33)-C(34)	115.4(2)
C(32)-C(33)-C(34)	122.9(3)
C(33)-C(34)-H(34A)	109.5
C(33)-C(34)-H(34B)	109.5
H(34A)-C(34)-H(34B)	109.5
C(33)-C(34)-H(34C)	109.5
H(34A)-C(34)-H(34C)	109.5
H(34B)-C(34)-H(34C)	109.5
O(4)-C(35)-N(2)	119.7(3)
O(4)-C(35)-C(36)	122.0(3)
N(2)-C(35)-C(36)	118.3(3)
C(35)-C(36)-H(36A)	109.5
C(35)-C(36)-H(36B)	109.5
H(36A)-C(36)-H(36B)	109.5
C(35)-C(36)-H(36C)	109.5
H(36A)-C(36)-H(36C)	109.5
H(36B)-C(36)-H(36C)	109.5
F(3)-B(2)-F(4)	111.5(3)
F(3)-B(2)-O(5)	108.9(3)
F(4)-B(2)-O(5)	108.1(3)
F(3)-B(2)-O(6)	109.1(3)
F(4)-B(2)-O(6)	107.9(3)

O(5)-B(2)-O(6)   111.3(2)

_____

Symmetry transformations used to generate equivalent atoms:

References

[S1] J. C. de Mello, H. F. Wittmann, R. H. Friend, Adv. Mater. 1997, 9, 230.

[S2] M. J. Frisch, G. W. Trucks, H. B. Schlegel, G. E. Scuseria, M. A. Robb, J. R. Cheeseman, G. Scalmani, V. Barone, G. A. Petersson, H. Nakatsuji, X. Li, M. Caricato, A. V. Marenich, J. Bloino, B. G. Janesko, R. Gomperts, B. Mennucci, H. P. Hratchian, J. V. Ortiz, A. F. Izmaylov, J. L. Sonnenberg, D. Williams-Young, F. Ding, F. Lipparini, F. Egidi, J. Goings, B. Peng, A. Petrone, T. Henderson, D. Ranasinghe, V. G. Zakrzewski, J. Gao, N. Rega, G. Zheng, W. Liang, M. Hada, M. Ehara, K. Toyota, R. Fukuda, J. Hasegawa, M. Ishida, T. Nakajima, Y. Honda, O. Kitao, H. Nakai, T. Vreven, K. Throssell, J. A. Montgomery, Jr., J. E. Peralta, F. Ogliaro, M. J. Bearpark, J. J. Heyd, E. N. Brothers, K. N. Kudin, V. N. Staroverov, T. A. Keith, R. Kobayashi, J. Normand, K. Raghavachari, A. P. Rendell, J. C. Burant, S. S. Iyengar, J. Tomasi, M. Cossi, J. M. Millam, M. Klene, C. Adamo, R. Cammi, J. W. Ochterski, R. L. Martin, K. Morokuma, O. Farkas, J. B. Foresman, and D. J. Fox, Gaussian 16, Revision B.01, Gaussian, Inc., Wallingford CT, 2016.